

Two-Electron-One-Photon Processes Can Dominate over Allowed Radiative and Auger Decay in Few-Electron Ions

M. Togawa,^{1,*} S. Kühn,^{1,2} C. Shah,^{1,3} P. Amaro,⁴ R. Steinbrügge,⁵ J. Stierhof,⁶ N. Hell,⁷ M. Rosner,^{1,2} K. Fujii,⁸ M. Bissinger,⁶ R. Ballhausen,⁶ M. Hoesch,⁵ J. Seltmann,⁵ S. Park,⁹ F. Grilo,⁴ F. S. Porter,³ J. P. Santos,⁴ M. Chung,⁹ T. Stöhlker,^{10,11,12} J. Wilms,⁶ T. Pfeifer,¹ G. V. Brown,⁷ M. A. Leutenegger,³ S. Bernitt,^{1,11,10,12} and J. R. Crespo López-Urrutia^{1,†}

¹*Max-Planck-Institut für Kernphysik, Saupfercheckweg 1, 69117 Heidelberg, Germany*

²*Heidelberg Graduate School of Fundamental Physics, Ruprecht-Karls-Universität Heidelberg, Im Neuenheimer Feld 226, 69120 Heidelberg, Germany*

³*NASA Goddard Space Flight Center, 8800 Greenbelt Rd, Greenbelt, MD 20771, USA*

⁴*Laboratory of Instrumentation, Biomedical Engineering and Radiation Physics (LIBPhys-UNL), Department of Physics, NOVA School of Science and Technology, NOVA University Lisbon, 2829-516 Caparica, Portugal*

⁵*Deutsches Elektronen-Synchrotron DESY, Notkestraße 85, 22607 Hamburg, Germany*

⁶*Dr. Karl Remeis-Sternwarte and Erlangen Centre for Astroparticle Physics, Sternwartstraße 7, 96049 Bamberg, Germany*

⁷*Lawrence Livermore National Laboratory, 7000 East Ave, Livermore, CA 94550, USA*

⁸*Department of Mechanical Engineering and Science,*

Graduate School of Engineering, Kyoto University, Kyoto 615-8540, Japan

⁹*Ulsan National Institute of Science and Technology, 50 UNIST-gil, Ulsan, South Korea*

¹⁰*Institut für Optik und Quantenelektronik, Friedrich-Schiller-Universität Jena, Fürstengraben 1, 07743 Jena, Germany*

¹¹*GSI Helmholtzzentrum für Schwerionenforschung, Planckstraße 1, 64291 Darmstadt, Germany*

¹²*Helmholtz-Institut Jena, Fröbelstieg 3, 07743 Jena, Germany*

(Dated: March 16, 2020)

We resonantly excite the K series of O^{5+} and O^{6+} up to principal quantum number $n = 11$ with monochromatic x rays, producing K -shell holes, and observe their relaxation by soft x-ray emission. Some photoabsorption resonances of O^{5+} reveal strong two-electron-one-photon (TEOP) transitions. We find that for the $1s2s5p^1P_1$ state, TEOP relaxation is by far stronger than the competing, and usually much faster, allowed Auger and radiative decay paths. This enhanced TEOP decay arises from a strong correlation with the near-degenerate upper state $1s2p4s^1P_1$ of a $K\alpha$ satellite. Even in three-electron systems, TEOP transitions can play a dominant role, and the present results should guide further research on the ubiquitous and abundant many-electron ions where various electronic energy degeneracies and level mixings are far more common.

In hot astrophysical plasmas, the most common elements, hydrogen and helium, are fully ionized, and only those with higher nuclear charge can keep some bound electrons, appearing as highly charged ions (HCI) [1]. The widths, Doppler shifts and relative intensities of their characteristic lines are recorded by x-ray observatories and analyzed for plasma diagnostics, relying not only on tabulated calculations but also on more scarce laboratory data. To fully exploit the data of present and upcoming high-resolution x-ray missions such as *XRISM* [2] and *ATHENA* [3], more accurate laboratory tests of the atomic models used in astrophysics are needed [1, 4]. Light elements such as carbon, nitrogen, and the here studied oxygen abundantly appear as HCI over a broad range of temperatures, and can thus serve as unique spectroscopic probes of, e. g., the warm-hot-intergalactic-medium (WHIM), which is critical to a complete census of baryonic matter in the Universe [5–7]. It is important to have good knowledge of both the photoabsorption cross sections and the various decay channels that govern the fluorescence yield and the ionization balance in plasmas. After x-ray absorption takes place, the most common relaxation processes are direct radiative decay

and autoionization. However, even in few-electron systems, more complex processes and multi-electron transitions also compete with them. Including such mechanisms in models is computationally intensive, and hence laboratory data are needed to guide those efforts [8].

Many-electron processes are intensively studied in both theory and experiment, and there is a plethora of recent examples on various subjects: multiple photodetachment of anions (see e. g., [9–12] and references therein); photoionization of atoms and ions [13–17] near inner-shell absorption edges [18–21]; and higher-order relaxation processes [22]. This also applies to ions (see e. g., [23, 24], HCI [25–27] and their interactions with free-electron lasers [28, 29]. Photorecombination also triggers multi-electronic excitations through resonant dielectronic [30–32], trielectronic and quadruelectronic processes [33–35]. The complexity of interelectronic correlations already within the L shell [15, 36–38] forces theoreticians to use approximations with uncertainties that are hard to benchmark in absence of laboratory data. As an example, the crucial determination of the cosmic abundance and column-density of O^{5+} in the WHIM suffers from large theoretical uncertainties [7, 39–41].

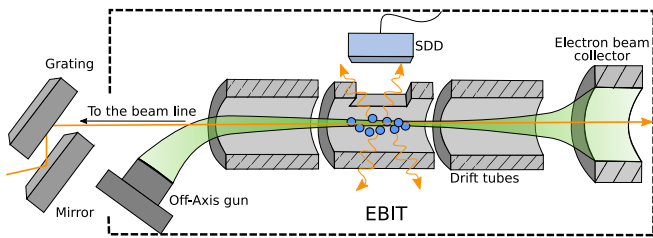


FIG. 1. Schematic of PolarX EBIT [43]. An electron beam from an off-axis gun is focused by a magnetic field and passes through drift tubes, where it generates and traps highly charged ions before reaching a collector electrode. A monochromatic photon beam enters axially and excites the trapped ions. The energies of fluorescence photons are recorded by a silicon-drift detector (SDD).

Here, we report on resonant excitation of the K series of He-like and Li-like oxygen ions between 570 and 750 eV using monoenergetic soft x rays. We detect their fluorescence-photon yield and energy as a function of the incident photon energy, and observe surprisingly strong and sometimes dominating two-electron-one-photon (TEOP) transitions in Li-like oxygen.

Our experiment was conducted at the variable-polarization XUV beamline P04 [42] of the PETRA III synchrotron facility with a portable electron beam ion trap (EBIT), PolarX [43] (see Fig. 1). Molecular oxygen was injected into the EBIT, dissociated and successively ionized yielding a large He-like O^{6+} population and a small Li-like O^{5+} fraction. These HCI are radially trapped by the electron beam (here 3 mA, to reduce ion heating), and axially confined within a potential well formed by making the central drift tube slightly more negative than the adjacent ones. With an electron-beam energy of ~ 200 eV just above the Li-like ionization threshold, we produce He-like O^{6+} , but stay below the excitation threshold of $K\alpha$ or higher K series transitions. This ensures a low-background measurement of the K series fluorescence by a silicon-drift detector (SDD) mounted side-on above the central drift tube where the ions are confined.

The P04 beamline is equipped with an APPLE-II undulator covering the photon energy range 250 to 3000 eV, and a grating monochromator (1200 lines/mm) providing circularly polarized light at a resolving power of more than 10^4 [42]. Expected long-time drifts of the monochromator recommended for this overview measurement a fast-scan mode lasting less than one hour, forcing the use of a wide slit ($100 \mu\text{m}$) for better statistics. This gave us a photon flux on the order of 10^{12} photons/s at a moderate resolving power. Nonetheless, we could determine excitation energies with a relative uncertainty of $\Delta E/E \approx 10^{-5}$. For this, we digitize the SDD-energy signal (y -axis) for each photon-detection event while con-

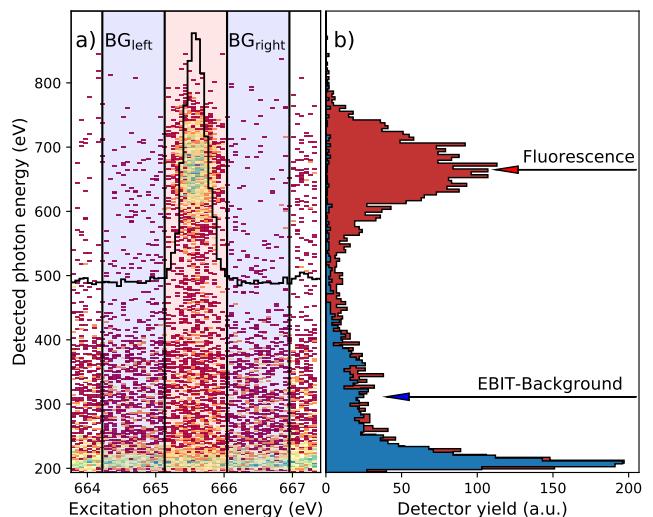


FIG. 2. a) Fluorescence yield (recorded by the SDD) of He-like $O^{6+} K_{\beta}$ under excitation with 663–668 eV photons (x -axis) versus fluorescence-photon energy (y -axis), and (black curve) projection of the photon yield onto x . b) Projections onto the y -axis of on/off resonance slices (red/blue histograms). The off-projection is used for subtraction of electron-induced background and SDD-noise.

tinuously scanning the monochromator, i. e., the incident photon energy (x -axis), obtaining a two-dimensional fluorescence histogram. To remove background events due to electron-impact excitation and recombination processes, we subtract at each resonance the off-resonance mean count rate from the on-resonance signal (see an example in Fig. 2). Then, we project the region of interest containing the resonance onto both axes, and fit Gaussians with a full-width-at-half-maximum of ~ 350 meV (x -axis) and ~ 100 eV (y -axis) to those projections.

A monochromator scan from 570 eV to 750 eV at 500 meV s^{-1} resolved the core excited K series of He-like oxygen up to $K\kappa$, as well as several other weaker Li-like resonances (Fig. 3). After determining the centroid positions of the six transitions $K\alpha$ up to $K\zeta$ on the approximately calibrated incident photon-energy scale (x -axis in Fig. 3), we assign them energies taken from accurate calculations by Yerokhin and Surzhykov [44] with uncertainties on the order of 0.5 meV, and determine the final monochromator-dispersion curve (see Supplementary Material). Its confidence interval is basically dominated by the ~ 20 meV statistical uncertainties of the individual transitions in our fast overview scan. For the SDD fluorescence-photon energy calibration we also use the K series transitions of He-Like oxygen (Fig. 3a) up to $K\zeta$, which show only direct decay (DD) to the ground state, assigning to the centroids of their y projections their respective energies.

Now we turn our attention to Li-like O^{5+} , a very essential astrophysical ion. Usually, inner-shell vacancies

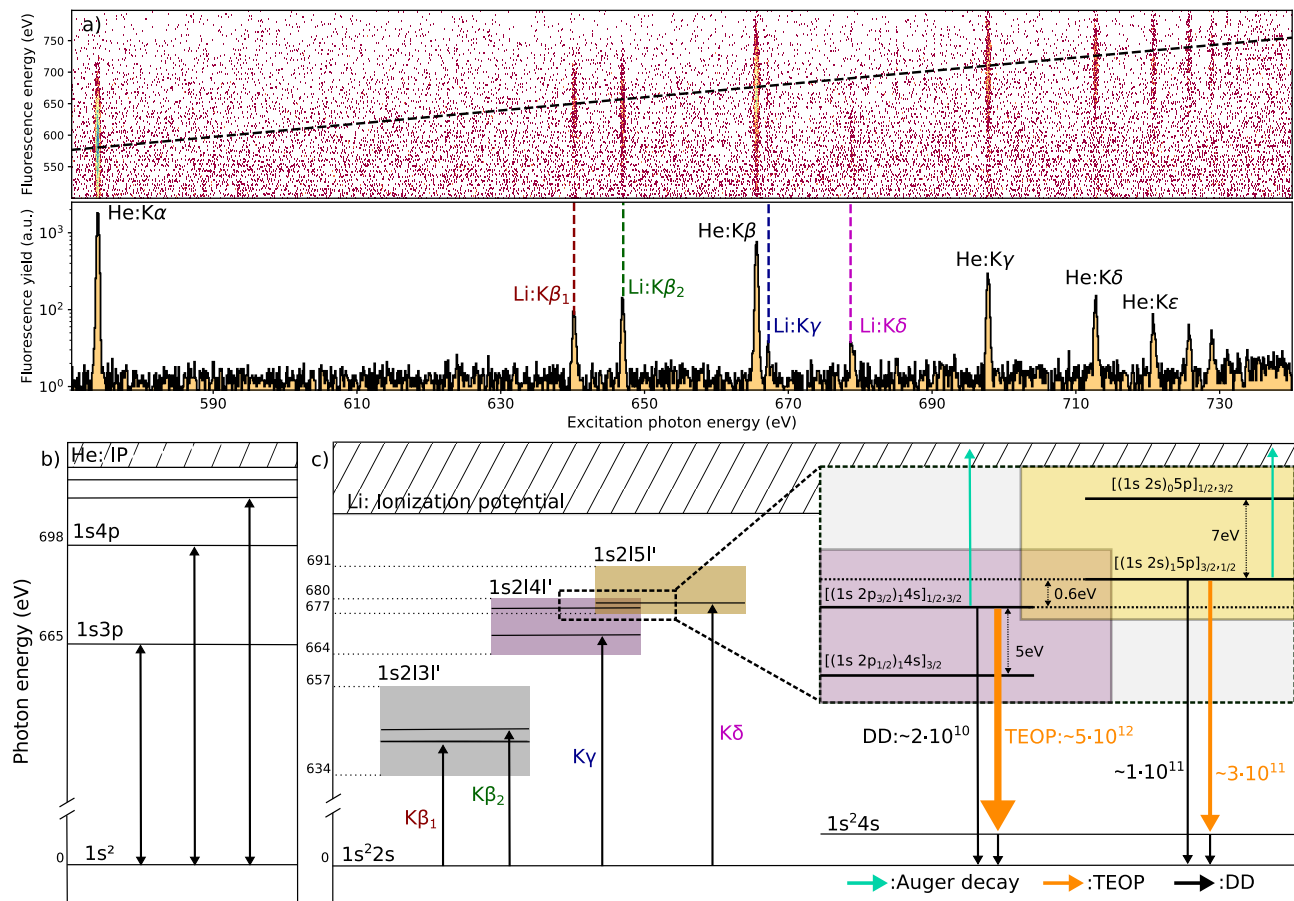


FIG. 3. **a)** (Top) Histogram of events registered with a silicon-drift detector (SDD): Fluorescence photon energy (y -axis) versus excitation photon energy (x -axis). (Bottom) Fluorescence from resonantly photoexcited He-like O^{6+} and Li-like O^{5+} , labeled in black and in color, respectively. Dashed line: Elastic channels, with excitation and fluorescence photon at equal energy. **b)** He-like and **c)** Li-like level diagrams. Mixing of the upper levels of $K\gamma$ and $K\delta$ causes a predominance of the TEOP process over both the direct-photonic relaxation and the Auger channels.

relax into the ground state by Auger decay (AD) emitting electrons, by one-electron-one-photon (OEOP) transitions, or cascades thereof. However, TEOP processes are possible, albeit at usually slower rates than the other processes. Multi-electron transitions were first considered in 1925 by W. Heisenberg [45], while Condon [46], Goudsmit and Gropper [47] found in 1931 the pertinent selection rules. More than forty years later, Wölfl *et al.* [48] observed TEOP x-ray photons following production of multiple inner-shell vacancies in heavy-ion-atom collisions. Later, they were seen in ion-ion collision [49–55] and EBIT experiments [56]. Various approaches for calculating transition rates and cross sections were introduced [57–63]. In general, they were regarded as second-order processes that could only be noticeable when otherwise competing OEOP transitions and AD were forbidden [36, 56, 64–66]. Here, in contrast, TEOP transitions suppress those other, usually dominant decay channels.

We measure the TEOP-transition energies in fluorescence to distinguish them from other channels. For both

Li-like $K\beta_1$ at 640 eV and $K\gamma$ at 666 eV, we observed a direct photo-de-excitation (PD) channel into the ground state: $1s2s3p \rightarrow 1s^22s$ and $1s2s4p \rightarrow 1s^22s$. This is apparent in the de-excitation spectrum of Fig. 3a, and corresponds to the elastic fluorescence transition. Fig. 4 shows the de-excitation spectra for $K\beta_1$ and $K\gamma$, confirming these elastic channels. However, as also displayed in Fig. 4, the 646 eV $K\beta_2$ line and $K\delta$ both reveal different de-excitation channels besides the expected elastic fluorescence. While $K\beta_2$ appears to have a minor contribution to the main elastic channel, $K\delta$ shows a dominant inelastic channel and no elastic one. To understand this, we performed calculations of the main de-excitation channels of the lines presented in Fig. 4 with the Flexible Atomic Code (FAC) [67], which provide us with transition rates which are missing in the high-accuracy calculations of Yerokhin and Surzhykov [44]. Our FAC results only include a limited number of configurations and thus show uncertainties on the order of 1 eV.

While doubly-excited states commonly relax by AD,

our FAC calculations show that this channel is only relevant for $K\beta_1$ and $K\gamma$ (see Fig. 5) and also confirm a main elastic DD channel for $K\beta_1$ and $K\gamma$. $K\beta_2$ has besides the DD elastic channel also TEOP channels feeding into the $1s^2 3s$ and $1s^2 3d$ states with higher transition rates than AD. The full de-excitation path consists of TEOP followed by radiative cascades (indicated with dots):

$$1s 2s 3p \xrightarrow{\text{TEOP}} 1s^2 3d \text{ (or } 3s) \rightarrow \dots \rightarrow 1s^2 2s$$

Mixing of $1s 2s 3p$ with $1s 2p 3s$ and $1s 2p 3d$ states leads to two TEOP channels roughly 5 eV apart (Fig. 3c). They feed corresponding $K\alpha$ satellites finally populating $1s^2 3s$ and $1s^2 3d$ states, and from there decay to the ground state through slow relaxation channels and cascades that sometimes include $E1$ -forbidden transitions. Photons emitted in these steps have too-low energies for detection with the SDD.

$K\delta$ exhibits no direct radiative de-excitation path. Here, the upper state dominantly relaxes through a TEOP transition to the $1s^2 4s$ state:

$$1s 2s 5p \xrightarrow{\text{TEOP}} 1s^2 4s \rightarrow \dots \rightarrow 1s^2 2s$$

The question is, what makes the usual direct photo de-excitation path to the ground state so weak. As shown in Fig. 3, the excited $1s 2s 5p$ state has a near-degeneracy (0.6 eV) with a state of same total angular momentum and parity, $1s 2p 4s$, which is also the upper state of a Li-like satellite of the He-like $K\alpha$ line. Thus, the excited states strongly mix with these, which have much higher

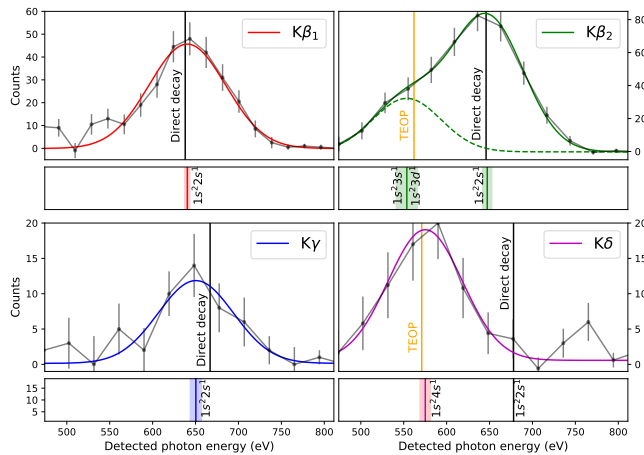


FIG. 4. Fitted fluorescence de-excitation spectra of the $K\beta_{1,2}$, $K\gamma$ and $K\delta$ absorption resonances in Li-like O^{5+} ions. Lines in the same color as the fit curves mark the corresponding de-excitation energies, and the shaded area their uncertainties. The respective final configuration appear next to their corresponding de-excitation energies. Orange line: theoretical TEOP channel position. Black line: theoretical direct decay channel position.

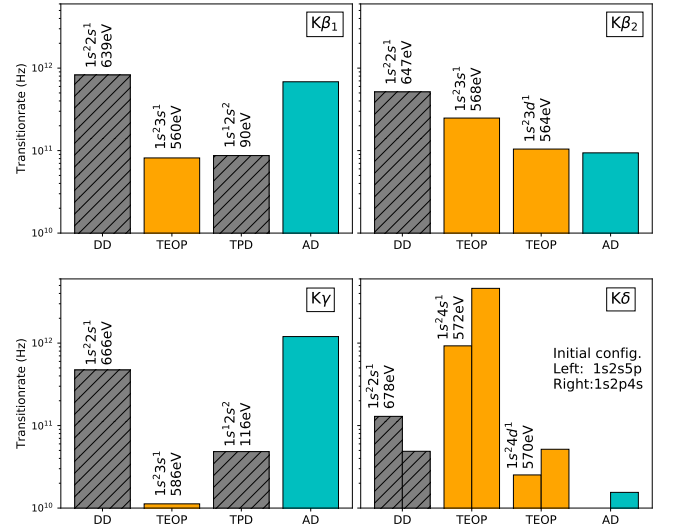


FIG. 5. FAC transition rate calculations for the strongest decay channels following resonant photoexcitation of the $K\beta_{1,2}$, $K\gamma$ and $K\delta$ in O^{5+} ions. Final states and transition energies are noted. DD: direct one-photon decay to the ground state; TEOP: two-electron-one photon decay; TPD: two-photon decay cascade; AD: Auger decay.

TABLE I. Core-hole relaxation following $K\beta_{1,2}$, $K\gamma$ and $K\delta$ resonant photon excitation in O^{5+} ions. First column: Excitation transition. Consecutive columns indicate for the decay channels their respective initial and final states, peak-photon energies (from silicon-drift detector), final-state energies (from FAC [67] calculations), and transition type (DD: direct photon decay; TEOP: two-electron-one-photon). Energies given in eV.

Line	Initial st.	Final st.	Photon energy	FAC	Type
$K\beta_1$	$1s 2s 3p$	$1s^2 2s$	639.0(4.5)	638.89	DD
$K\beta_2$	$1s 2s 3p$	$1s^2 2s$	639.8(6.0)	645.98	DD
$K\beta_2$	$1s 2s 3p$	$1s^2 3s$	542.0(17.5)	566.68	TEOP
		$1s^2 3d$	blend	562.26	TEOP
$K\gamma$	$1s 2s 4p$	$1s^2 2s$	650.2(7.8)	655.58	DD
$K\delta$	$1s 2s 5p$	$1s^2 4s$	574.9(7.6)	571.53	TEOP

decay rates towards $1s^2 4s$ (on the order of 10^{12} s^{-1}). This suppresses the direct one-photon relaxation to the ground state, as can be seen in Fig. 4. The measured de-excitation energies are listed in Tab. I. While the de-excitation channels can be clearly separated, the centroids of the energy-resolved fluorescence were only determined with an uncertainty in the 1–3% range due to insufficient statistics; this will be easily improved in the future, e. g., with an x-ray microcalorimeter [68] also resolving the $K\beta_2$ channels.

Although a strong suppression of the direct photo decay by TEOP transitions was observed in just one of several lines in Li-like oxygen, it is not far-fetched to assume that TEOP-dominated relaxation also happens in other multiply excited, multi-electron systems, and thus

its contribution should not be neglected in accurate astrophysical plasma models. The upcoming launches of *XRISM* [2] and *ATHENA* [3] urgently call for studying position and strength of TEOP transitions that can cause shifts, or broaden the strong diagnostically important O-*K* and Fe-*L* lines in the 15–23 Å range, which are crucial for determining gas-outflow velocities of warm absorbers and density diagnostics of photoionized plasmas [36, 69–72], and needed for accurately modeling the x-ray continuum flux.

We have demonstrated that a complex process which is difficult to disentangle in astrophysical plasmas can be isolated and studied in detail by high-resolution photon excitation. Unexpectedly strong TEOP transitions were found in an essential species, the relatively simple Li-like O⁺⁵, showing, among other observations, evidence that the upper state of the *Kδ* line in Li-like O⁺⁵ mainly de-excites as a satellite of He-like O⁺⁶ *Kα*. This produces a problematic blend in a key feature for the diagnostics of photoionized plasmas (e.g. [72]). Systems with more than three electrons have richer overlapping excitations with manifold decay channels that do not only cause similar blends in emission and absorption spectra, but also affect the ionization balance of plasmas. The here studied three-electron system is better tractable by current theory and allowed us stringently testing the underlying electronic correlations.

ACKNOWLEDGEMENTS

Financial support was provided by the Max-Planck-Gesellschaft (MPG) and Bundesministerium für Bildung und Forschung (BMBF) through project 05K13SJ2. We acknowledge DESY (Hamburg, Germany), a member of the Helmholtz Association HGF, for the provision of experimental facilities. Parts of this research were carried out at PETRAIII. Work by C. S. was supported by the Deutsche Forschungsgemeinschaft (DFG) Project No. 266229290 and by an appointment to the NASA Postdoctoral Program at the NASA Goddard Space Flight Center, administered by Universities Space Research Association under contract with NASA. P. A. acknowledges the support from Fundação para a Ciência e a Tecnologia (FCT), Portugal, under Grant No. UID/FIS/04559/2020(LIBPhys) and under Contract No. SFRH/BPD/92329/2013. Work by UNIST was supported by the National Research Foundation of Korea (No. NRF-2016R1A5A1013277). Work by LLNL was performed under the auspices of the U. S. Department of Energy under Contract No. DE-AC52-07NA27344 and supported by NASA grants to LLNL. M. A. L. and F. S. P. acknowledge support from NASAs Astrophysics Program.

SUPPLEMENTARY MATERIAL

EXPERIMENTAL EXCITATION ENERGIES

The centroids of the observed resonances of He and Li-like oxygen (see Fig. 3a) were determined by a least-squares fit of a gaussian profile to the region of interest. As briefly explained above the theory values of He-like oxygen were used to determine a dispersion curve, which was used to calibrate the centroid values. In table II the experimental values and available theory values are put together.

DETERMINATION OF THE IONIZATION POTENTIAL OF HE-LIKE OXYGEN

For the determination of the ionization potential of O⁶⁺, we use a simple model based on the Rydberg formula and a quantum defect, with the Rydberg energy E_R , the effective nuclear charge Z_{eff} and the quantum defect $\delta_{n,l}$ for principal n respectively orbital l quantum numbers:

$$\begin{aligned} K_n &= Z_{\text{eff}}^2 E_R \left((1 - \delta_{1,s})^{-2} - (n - \delta_{n,l})^{-2} \right), \\ &= E_{IP} - Z_{\text{eff}}^2 E_R (n - \delta_{n,l})^{-2}. \end{aligned}$$

By extrapolation of the monochromator-dispersion relation, we determined the excitation energies of the *Kη*, *Kθ*, *Kι* and *Kκ* transitions (see Tab. I), and inferred the ionization potential (IP) of O⁶⁺ with a fit to the measured *K*-series to be IP = 739.327 ± 0.016 eV. This agrees very well with the prediction of Drake [74], 739.32682(6) eV, see Tab. II.

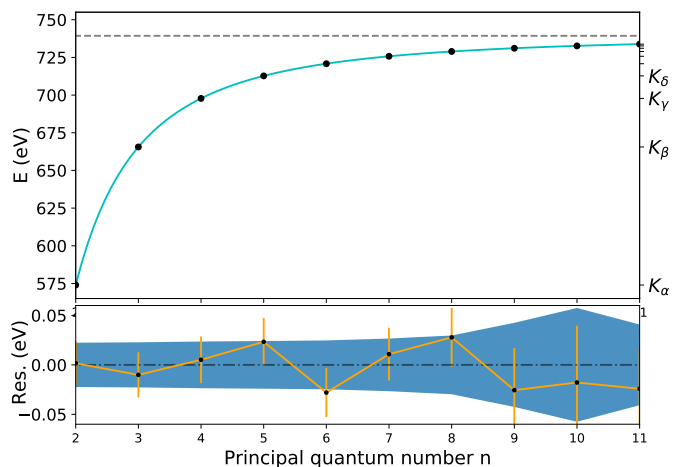


FIG. 6. Fit of Rydberg formula to measured He-like *K*-series with nuclear effective charge Z_{eff} and quantum defect δ as free parameter. The blue shaded are indicates the confidence interval.

TABLE II. Experimental excitation energies of He-like and Li-like oxygen absorption resonances. Measured energy differences (ΔE) to the uncalibrated He-like $K\alpha$ are referenced to the theoretical value of that transition given by Yerokhin in [44] in order to obtain their absolute energy (absolute E), and compared to other available calculations and the NIST ASD database [73]. Energies are given in units of eV.

Ion	Label	Final configuration	Absolute E	QED theory [44]	NIST [73]
O VII	$K\alpha$	$[1s_{1/2} 2p_{3/2}]_1$	573.96(2)	573.9614(5)	573.9478
O VII	$K\beta$	$[1s_{1/2} 3p_{3/2}]_1$	665.58(2)	665.5743(3)	665.6154
O VII	$K\gamma$	$[1s_{1/2} 4p_{3/2}]_1$	697.79(2)	697.7859(3)	697.7955
O VII	$K\delta$	$[1s_{1/2} 5p_{3/2}]_1$	712.74(2)	712.7221(3)	712.717
O VII	$K\epsilon$	$[1s_{1/2} 6p_{3/2}]_1$	720.81(2)	720.8434(3)	720.8379
O VII	$K\zeta$	$[1s_{1/2} 7p_{3/2}]_1$	725.75(3)	725.7432(3)	725.6473
O VII	$K\eta$	$[1s_{1/2} 8p_{3/2}]_1$	728.95(3)		
O VII	$K\theta$	$[1s_{1/2} 9p_{3/2}]_1$	731.08(4)		
O VII	$K\iota$	$[1s_{1/2} 10p_{3/2}]_1$	732.65(6)		
O VII	$K\kappa$	$[1s_{1/2} 11p_{3/2}]_1$	733.80(4)		
<hr/>					
O VI	$K\beta_1$	$[(1s 2s)_1 3p_{3/2}]_{3/2;1/2}$	640.20(2)		
O VI	$K\beta_2$	$[(1s 2s)_0 3p_{1/2,3/2}]_{1/2;3/2}$	646.96(2)		
O VI	$K\gamma$	$[(1s 2s)_1 4p_{3/2}]_{3/2;1/2}$	667.18(3)		
O VI	$K\delta$	$[(1s 2s)_1 5p_{3/2}]_{3/2;1/2}$	678.90(4)		

TABLE III. Fit results in comparison with available theoretical and experimental values.

	Fit	J.Scofield [75]	NIST [74]
IP	739.336(16)	739.3	739.32682(6)
Z_{eff}	7.008(3)		
δ	-0.0014(9)		

BACKGROUND REMOVAL FROM SILICON-DRIFT DETECTOR SIGNAL

Background removal procedure. The mean count rate per channel outside a resonance ($N_{\text{BG}_{\text{left}}}, N_{\text{BG}_{\text{right}}}$ is subtracted from each bin N in the de-excitation spectrum of the resonance, resulting in a effective count rate N' with error $\Delta N'$.

$$N' = N - \frac{N_{\text{BG}_{\text{left}}} + N_{\text{BG}_{\text{right}}}}{2}$$

$$\Delta N' = \sqrt{N + \frac{1}{4}(N_{\text{BG}_{\text{left}}} + N_{\text{BG}_{\text{right}}})}$$

* moto.togawa@mpi-hd.mpg.de

† crespj@mpi-hd.mpg.de

- [1] P. Beiersdorfer, *Annual Review of Astronomy and Astrophysics* **41**, 343 (2003).
[2] M. Tashiro, H. Maejima, K. Toda, R. Kelley, L. Reichen-thal, J. Lobell, R. Petre, M. Guainazzi, E. Costantini, M. Edison, *et al.*, *Proc. SPIE* **10699**, 1069922 (2018).

- [3] D. Barret, T. L. Trong, J.-W. Den Herder, L. Piro, X. Barcons, J. Huovelin, R. Kelley, J. M. Mas-Hesse, K. Mitsuda, S. Paltani, *et al.*, in *Space Telescopes and Instrumentation 2016: Ultraviolet to Gamma Ray*, Vol. 9905 (International Society for Optics and Photonics, 2016) p. 99052F.
[4] N. Hell, P. Beiersdorfer, G. V. Brown, M. E. Eckart, R. L. Kelley, C. A. Kilbourne, M. A. Leutenegger, T. E. Lockard, F. S. Porter, and J. Wilms, *X-Ray Spectrometry* **49**, 218 (2020).
[5] R. A. Simcoe, W. L. W. Sargent, and M. Rauch, *Astrophys. J* **578**, 737 (2002).
[6] F. Nicastro, J. Kaastra, Y. Krongold, S. Borgani, E. Branchini, R. Cen, M. Dadina, C. W. Danforth, M. Elvis, F. Fiore, *et al.*, *Nature* **558**, 406 (2018).
[7] E. Gatuzz, J. A. García, and T. R. Kallman, *Mon. Not. R. Astron. Soc.* **483**, L75 (2018).
[8] T. R. Kallman and P. Palmeri, *Rev. Mod. Phys.* **79**, 79 (2007).
[9] T. Gorczyca, *Radiat. Phys. Chem.* **70**, 407 (2004).
[10] S. Schippers, R. Beerwerth, L. Abrok, S. Bari, T. Buhr, M. Martins, S. Ricz, J. Viefhaus, S. Fritzsche, and A. Müller, *Phys. Rev. A* **94**, 041401(R) (2016).
[11] A. Müller, A. Borovik, S. Bari, T. Buhr, K. Holste, M. Martins, A. Perry-Saßmannshausen, R. A. Phaneuf, S. Reinwardt, S. Ricz, *et al.*, *Phys. Rev. Lett.* **120**, 133202 (2018).

- [12] A. Perry-Sassmannshausen, T. Buhr, A. Borovik, M. Martins, S. Reinwardt, S. Ricz, S. O. Stock, F. Trinter, A. Müller, S. Fritzsche, and S. Schippers, *Phys. Rev. Lett.* **124**, 083203 (2020).
- [13] J. B. West, *J. Phys. B: At., Mol. Opt. Phys.* **34**, R45 (2001).
- [14] H. Kjeldsen, *J. Phys. B: At., Mol. Opt. Phys.* **39**, R325 (2006).
- [15] J. M. Bizau, D. Cubaynes, S. Guilbaud, M. M. Al Shorman, M. F. Gharaibeh, I. Q. Ababneh, C. Blancard, and B. M. McLaughlin, *Phys. Rev. A* **92**, 023401 (2015).
- [16] N. Berrah, J. Bozek, R. Bilodeau, and E. Kukk, *Radiat. Phys. Chem.* **70**, 57 (2004), photoeffect: Theory and Experiment.
- [17] M. F. Gharaibeh, A. Aguilar, A. M. Covington, E. D. Emmons, S. W. J. Scully, R. A. Phaneuf, A. Müller, J. D. Bozek, A. L. D. Kilcoyne, A. S. Schlachter, *et al.*, *Phys. Rev. A* **83**, 043412 (2011).
- [18] J. C. Levin and G. Armen, *Radiat. Phys. Chem.* **70**, 105 (2004), photoeffect: Theory and Experiment.
- [19] N. Kabachnik, S. Fritzsche, A. Grum-Grzhimailo, M. Meyer, and K. Ueda, *Phys. Rep.* **451**, 155 (2007).
- [20] S. H. Southworth, R. W. Dunford, D. Ray, E. P. Kanter, G. Doumy, A. M. March, P. J. Ho, B. Krässig, Y. Gao, C. S. Lehmann, *et al.*, *Phys. Rev. A* **100**, 022507 (2019).
- [21] Y. Ma, F. Zhou, L. Liu, and Y. Qu, *Phys. Rev. A* **96**, 042504 (2017).
- [22] R. Dunford, E. Kanter, B. Krässig, S. Southworth, and L. Young, *Radiat. Phys. Chem.* **70**, 149 (2004), photoeffect: Theory and Experiment.
- [23] S. Schippers, A. L. D. Kilcoyne, R. A. Phaneuf, and A. Miller, *Contemp. Phys.* **57**, 215 (2016).
- [24] A. Miller, D. Bernhardt, A. Borovik, T. Buhr, J. Hellhund, K. Holste, A. L. D. Kilcoyne, S. Klumpp, M. Martins, S. Ricz, *et al.*, *Astrophys. J* **836**, 166 (2017).
- [25] C. Blancard, D. Cubaynes, S. Guilbaud, and J.-M. Bizau, *Astrophys. J* **853**, 32 (2018).
- [26] M. C. Simon, J. R. Crespo López-Urrutia, C. Beilmann, M. Schwarz, Z. Harman, S. W. Epp, B. L. Schmitt, T. M. Baumann, E. Behar, S. Bernitt, *et al.*, *Phys. Rev. Lett.* **105**, 183001 (2010).
- [27] R. Steinbrügge, S. Bernitt, S. W. Epp, J. K. Rudolph, C. Beilmann, H. Bekker, S. Eberle, A. Müller, O. O. Versolato, H.-C. Wille, *et al.*, *Phys. Rev. A* **91**, 032502 (2015).
- [28] L. Young, E. P. Kanter, B. Krässig, Y. Li, A. M. March, S. T. Pratt, R. Santra, S. H. Southworth, N. Rohringer, L. F. DiMauro, *et al.*, *Nature* **466**, 56 (2010).
- [29] C. Buth, R. Beerwerth, R. Obaid, N. Berrah, L. S. Cederbaum, and S. Fritzsche, *J. Phys. B: At., Mol. Opt. Phys.* **51**, 055602 (2018).
- [30] P. Beiersdorfer, T. W. Phillips, K. L. Wong, R. E. Marrs, and D. A. Vogel, *Phys. Rev. A* **46**, 3812 (1992).
- [31] N. Nakamura, A. P. Kavanagh, H. Watanabe, H. A. Sakaue, Y. Li, D. Kato, F. J. Currell, and S. Ohtani, *Phys. Rev. Lett.* **100**, 73203 (2008).
- [32] C. Shah, H. Jörg, S. Bernitt, S. Dobrodey, R. Steinbrügge, C. Beilmann, P. Amaro, Z. Hu, S. Weber, S. Fritzsche, *et al.*, *Phys. Rev. A* **92**, 042702 (2015).
- [33] M. Schnell, G. Gwinner, N. R. Badnell, M. E. Bannister, S. Böhm, J. Colgan, S. Kieslich, S. D. Loch, D. Mitnik, A. Müller, *et al.*, *Phys. Rev. Lett.* **91**, 043001 (2003).
- [34] C. Beilmann, P. H. Mokler, S. Bernitt, C. H. Keitel, J. Ullrich, J. R. Crespo López-Urrutia, and Z. Harman, *Phys. Rev. Lett.* **107**, 143201 (2011).
- [35] C. Shah, P. Amaro, R. Steinbrügge, C. Beilmann, S. Bernitt, S. Fritzsche, A. Surzhykov, J. R. Crespo López-Urrutia, and S. Tashenov, *Phys. Rev. E* **93**, 061201(R) (2016).
- [36] J. J. Drake, D. A. Swartz, P. Beiersdorfer, G. V. Brown, and S. M. Kahn, *Astrophys. J* **521**, 839 (1999).
- [37] P. Liu, J. Zeng, and J. Yuan, *J. Phys. B: At., Mol. Opt. Phys.* **51**, 075202 (2018).
- [38] V. A. Zaytsev, I. A. Maltsev, I. I. Tupitsyn, and V. M. Shabaev, *Phys. Rev. A* **100**, 052504 (2019).
- [39] E. Behar, M. Sako, and S. M. Kahn, *Astrophys. J* **563**, 497 (2001).
- [40] B. M. McLaughlin, J.-M. Bizau, D. Cubaynes, S. Guilbaud, S. Douix, M. M. A. Shorman, M. O. A. E. Ghazaly, I. Sakho, and M. F. Gharaibeh, *Mon. Not. R. Astron. Soc.* **465**, 4690 (2016).
- [41] S. Mathur, F. Nicastro, A. Gupta, Y. Krongold, B. M. McLaughlin, N. Brickhouse, and A. Pradhan, *Astrophys. J* **851**, L7 (2017).
- [42] J. Vieffhaus, F. Scholz, S. Deinert, L. Glaser, M. Ilchen, J. Seltmann, P. Walter, and F. Siewert, *Nucl. Instrum. Methods Phys. Res.* **710**, 151 (2013), the 4th international workshop on Metrology for X-ray Optics, Mirror Design, and Fabrication.
- [43] P. Micke, S. Khn, L. Buchauer, J. R. Harries, T. M. Bcking, K. Blaum, A. Cieluch, A. Egl, D. Hollain, S. Kraemer, *et al.*, *Rev. Sci. Instrum.* **89**, 063109 (2018).
- [44] V. A. Yerokhin and A. Surzhykov, *J. Phys. Chem. Ref. Data* **48**, 033104 (2019).
- [45] W. Heisenberg, *Zeitschrift für Physik* **32**, 841 (1925).
- [46] E. U. Condon, *Phys. Rev.* **36**, 1121 (1930).
- [47] S. Goudsmit and L. Gropper, *Phys. Rev.* **38**, 225 (1931).
- [48] W. Wölffi, C. Stoller, G. Bonani, M. Suter, and M. Stöckli, *Phys. Rev. Lett.* **35**, 656 (1975).
- [49] J. P. Briand, P. Chevallier, A. Johnson, J. P. Rozet, M. Tavernier, and A. Touati, *Phys. Lett. A* **49**, 51 (1974).
- [50] E. Mikkola, O. Keski-Rahkonen, and R. Kuoppala, *Phys. Scr.* **19**, 29 (1979).
- [51] C. Stoller, W. Wölffi, G. Bonani, M. Stöckli, and M. Suter, *Phys. Rev. A* **15**, 990 (1977).
- [52] J. Ahopelto, E. Rantavuori, and O. Keski-Rahkonen, *Phys. Scr.* **20**, 71 (1979).
- [53] S. I. Salem, A. Kumar, B. L. Scott, and R. D. Ayers, *Phys. Rev. Lett.* **49**, 1240 (1982).
- [54] S. I. Salem, A. Kumar, and B. L. Scott, *Phys. Rev. A* **29**, 2634 (1984).
- [55] J. Auerhammer, H. Genz, A. Kumar, and A. Richter, *Phys. Rev. A* **38**, 688 (1988).
- [56] Y. Zou, J. R. Crespo López-Urrutia, and J. Ullrich, *Phys. Rev. A* **67**, 042703 (2003).
- [57] H. P. Kelly, *Phys. Rev. Lett.* **37**, 386 (1976).
- [58] T. Åberg, K. A. Jamison, and P. Richard, *Phys. Rev. Lett.* **37**, 63 (1976).
- [59] M. Gavrilin and J. E. Hansen, *J. Phys. B: At. Mol. Phys.* **11**, 1353 (1978).
- [60] G. B. Baptista, *J Phys B: At Mol Phys* **19**, 159 (1986).
- [61] T. K. Mukherjee and K. K. Ghosh, *Phys. Rev. A* **37**, 4985 (1988).
- [62] J. K. Saha, T. K. Mukherjee, S. Fritzsche, and P. K. Mukherjee, *Phys. Lett. A* **373**, 252 (2009).

- [63] R. Kadrekar and L. Natarajan, *J. Phys. B: At., Mol. Opt. Phys.* **43**, 155001 (2010).
- [64] P. Indelicato, *Hyperfine Interact.* **108**, 39 (1997).
- [65] S. Trotsenko, T. Stöhlker, D. Banas, C. Z. Dong, S. Fritzsche, A. Gumberidze, S. Hagmann, S. Hess, P. Indelicato, Kozhuharov, *et al.*, *J. Phys. Conf. Ser.* **58**, 141 (2007).
- [66] J. P. Marques, F. Parente, A. M. Costa, M. C. Martins, P. Indelicato, and J. P. Santos, *Phys. Rev. A* **86**, 052521 (2012).
- [67] M. F. Gu, *Can. J. Phys.* **86**, 675 (2008).
- [68] M. Durkin, J. S. Adams, S. R. Bandler, J. A. Chervakov, S. Chaudhuri, C. S. Dawson, E. V. Denison, W. B. Doriese, S. M. Duff, F. M. Finkbeiner, *et al.*, *IEEE Transactions on Applied Superconductivity* **29**, 2904472 (2019).
- [69] E. Behar, A. P. Rasmussen, A. J. Blustin, M. Sako, S. M. Kahn, J. S. Kaastra, G. Branduardi-Raymont, and K. C. Steenbrugge, *Astrophys. J* **598**, 232 (2003).
- [70] M. Schmidt, P. Beiersdorfer, H. Chen, D. B. Thorn, E. Trabert, and E. Behar, *Astrophys. J* **604**, 562 (2004).
- [71] M. F. Gu, M. Schmidt, P. Beiersdorfer, H. Chen, D. B. Thorn, E. Trabert, E. Behar, and S. M. Kahn, *Astrophys. J* **627**, 10661071 (2005).
- [72] M. Mehdipour, J. S. Kaastra, and A. J. J. Raassen, *Astron. Astrophys* **579**, A87 (2015).
- [73] A. Kramida, Yu. Ralchenko, J. Reader, and NIST ASD Team, NIST Atomic Spectra Database (ver. 5.7.1), [Online]. Available: <https://physics.nist.gov/asd> [2017, April 9]. National Institute of Standards and Technology, Gaithersburg, MD.
- [74] G. W. Drake, *Can. J. Phys.* **66**, 586 (1988).
- [75] J. Scofield, “X-ray data booklet,” (2009).